Nano Research

ISSN 1998-0124 CN 11-5974/O4
https://doi.org/10.1007/s12274-022-4423-2

Research Article

Polydopamine-assisted *in-situ* formation of dense MOF layer on polyolefin separator for synergistic enhancement of lithium-sulfur battery

Xiuxiu Wu[1,§], Cheng Zhou[1,§], Chenxu Dong[2], Chunli Shen[1], Binbin Shuai[1], Cheng Li[1], Yan Li[1], Qinyou An[1] (✉), Xu Xu[2] (✉), and Liqiang Mai[1]

[1] *State Key Laboratory of Advanced Technology for Materials Synthesis and Processing, Wuhan University of Technology, Wuhan 430070, China*
[2] *International School of Materials Science and Engineering, Wuhan University of Technology, Wuhan 430070, China*
[§] *Xiuxiu Wu and Cheng Zhou contributed equally to this work.*

Received: 16 February 2022 / **Revised:** 29 March 2022 / **Accepted:** 13 April 2022

ABSTRACT

The separator is of great significance to alleviate the shuttle effect and dendrite growth of lithium-sulfur batteries. However, most of the current commercial separators cannot meet these requirements well. In this work, a dense metal-organic-framework (MOF) modification layer is *in-situ* prepared by the assistant of polydopamine on the polypropylene separators. Due to the unique structure and synergistic effect of polydopamine (PDA) and zeolitic imidazolate framework-8 (ZIF-8), the functional separator can not only trap the polysulfides effectively but also promote the transport of lithium ions. As a result, the battery assembled with the functional separator exhibits excellent cycle stability. The capacity remains 711 mAh·g^{-1} after 500 cycles at 2 C, and the capacity decay rate is as low as 0.013% per cycle. The symmetrical battery is cycled for 1,000 h at 2 mA·cm^{-2} (2 mAh·cm^{-2}) with the plating/stripping overpotential of 20 mV. At the same time, the modification separator shows a higher lithium ion transference number (0.88), better thermal stability and electrolyte wettability than the unmodified separator.

KEYWORDS

metal-organic frameworks, *in-situ* growth, polysulfides, shuttle effect, gradient distribution

1 Introduction

With the increasing demand for energy storage technology, the energy density of commercial lithium-ion batteries has been in short supply. Among the new types of batteries, lithium-sulfur (Li-S) batteries stand out due to their theoretical capacity of up to 1,675 mAh·g^{-1} and energy density of 2,600 Wh·kg^{-1} [1, 2]. However, its commercialization is still hampered by a series of problems. Among them, the shuttle effect caused by the soluble polysulfides during charge and discharge, and the lithium dendrite caused by the nonuniform deposition of lithium ions are the most serious problems affecting the performance of Li-S batteries [3–5]. At present, various strategies have been used to solve the above problems, including electrode structure design, separator modification and electrolyte optimization [6–8].

As an important part placed between the anode and cathode to prevent the electrical short circuit, the separator provides channels for lithium ions to transport. Unfortunately, the existence of the pores with the site of tens of nanometers in the ummercial polyolefin separators also allows the shuttle of polysulfides [9]. And the unmodified polyolefin separator is inert to polysulfides, which cannot absorb the shuttle of polysulfides physically or chemically. Moreover, due to the poor wettability of the separator for electrolytes, the distribution of the electrolyte in the pores is affected, and it is difficult to form uniform and continuous lithium ion channels, which hinders the uniform transport of lithium ions [10, 11]. Therefore, the modification of the separator is of significance to restrain the shuttle of polysulfides and achieve uniform transport of lithium ions in Li-S batteries. In the past decade, a series of materials have been tried to modify separators. Initially, materials such as polymers [12, 13], graphene [14] and carbon nanotubes [15] were used as the modification layer to cover the separator pores to achieve the purpose of physical barrier. Later, researchers found that polar materials had chemisorption of polysulfides, such as metal oxides [16], metal nitrides [17], sulfide [18, 19], and metal-organic frameworks (MOFs) [20, 21], which can inhibit the shuttle of polysulfides through chemical adsorption. The results demonstrate that combining physical barrier and chemical adsorption has a better effect on inhibiting the shuttle of polysulfides [22–24].

MOFs equip with the advantages of high porosity, low density, adjustable pore size, etc., which are widely used in catalysis, energy storage, liquid phase separation and other directions [25–27]. In the field of separator modification of Li-S batteries, MOF materials containing unsaturated metal ions are mainly used to provide chemical adsorption sites, spontaneously adsorb anions to inhibit polysulfides shuttle and contribute to the effective transport of lithium ions in the electrolyte greatly. The effect of MOF materials on Li-S batteries has been demonstrated by a large number of experimental results [21, 27–29], but the existing problem is that it is difficult to form a robust modification layer on the surface of the

Address correspondence to Qinyou An, anqinyou86@whut.edu.cn; Xu Xu, xuxu@whut.edu.cn

flexible polypropylene (PP) separator through the commonly used preparation methods.

The vacuum filtration and roller coating are most commonly used methods in separator modification [30]. As the most mature commercial process at present, the thickness of the coating layers from the roller coating method is generally from a few to ten micrometers, which conspicuously increases the thickness of the separator and affects the energy density of the battery [31]. The modification layer prepared by vacuum filtration can reach a thinner layer [32]. However, it may cause the incomplete coverage of the modification layer on the pores [33]. Moreover, because the process of vacuum filtration does not add binders, it is easy to fall off during cycling for the modification material, seriously affecting the durability. Based on these problems, *in-situ* growth method is employed for the preparation of the robust modification layers, which has a closer and firmer contact with the separator. And the bottom-up growth method allows the thickness of the modification layer to be well controlled without affecting the degree of coverage of the pores [34]. Our group prepared a MOF-PAN/rGO-PAN (rGO = reduced graphene oxide and PAN = polyacrylonitrile) membrane by electrospinning and following low-pressure chemical vapor deposition method [35]. The *in-situ* grown MOF particles closely bind to PAN nanofibers and can adsorb polysulfides effectively. However, the employed methods are difficult to scale up and put into commercial production. Therefore, from the perspective of technical difficulty and industrialization, an *in-situ* growth method that can be put into mass production needs to be proposed.

Herein, a scheme of using polydopamine (PDA) as a "bridge" to achieve the *in-situ* growth of zeolitic imidazolate framework-8 (ZIF-8) on the PP separator is realized through the liquid phase method. First, the abundant functional groups of PDA provide strong adhesive force to combine the separator and ZIF-8 nanoparticles to form a dense ultra-thin layer on the separator (Fig. 1(a)). This ultra-thin and lightweight modification layer minimizes the burden on the volume and mass of the battery, and the firm adhesion realizes the high stability of the composite separator. Second, the abundant metal sites in ZIF-8 serve as adsorption sites to provide strong chemical adsorption capacity for polysulfides. The combination of the physical barrier and chemical adsorption provided by the dense modification layer can greatly alleviate the massive capacity loss caused by the shuttle effect. Third, the synergistic effect of PDA and ZIF-8 promotes the transmission of lithium ions, homogenizes the lithium ion flux, and alleviates the formation of lithium dendrite. Therefore, the separator modified by this method possesses better thermal

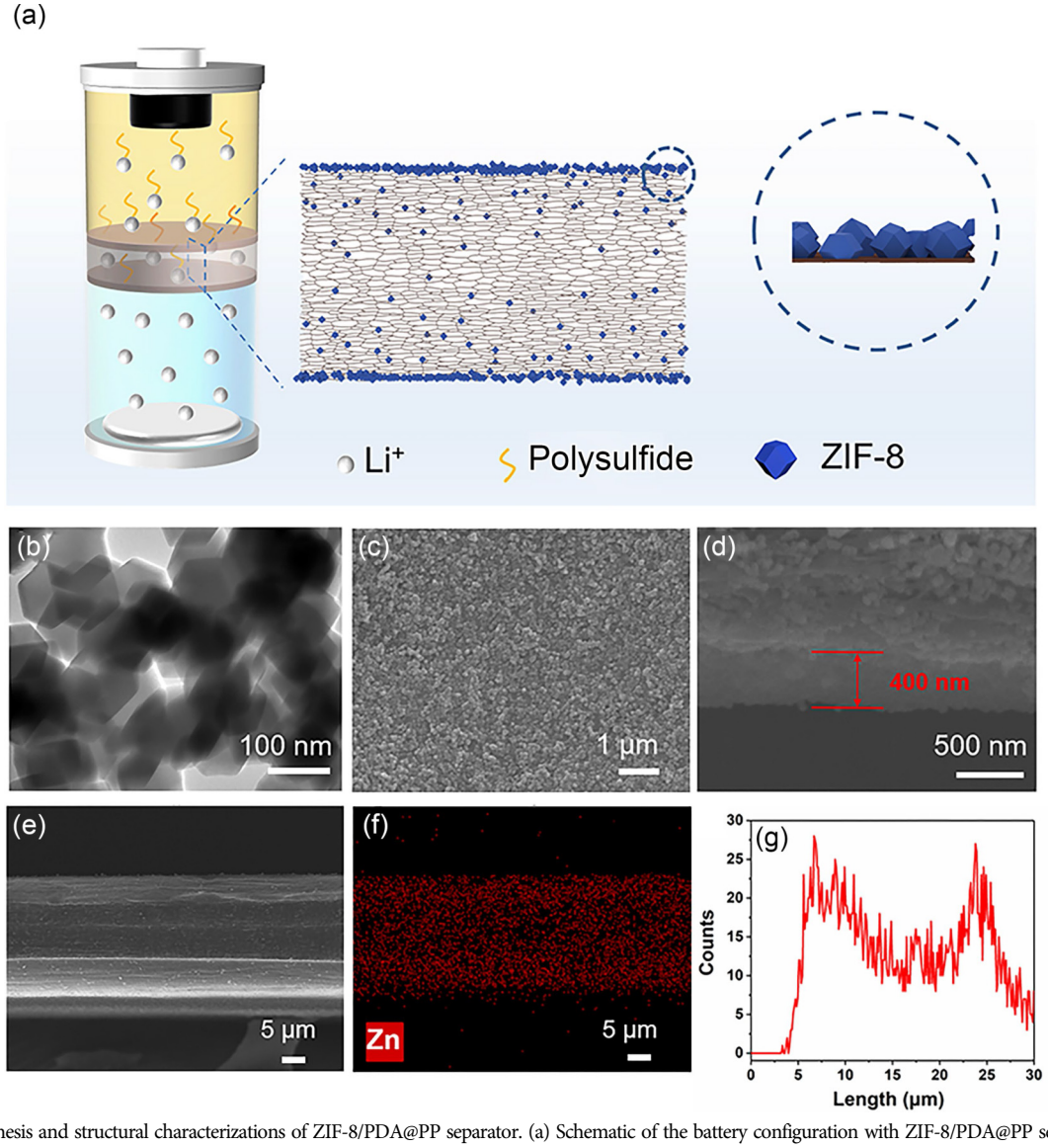

Figure 1 Synthesis and structural characterizations of ZIF-8/PDA@PP separator. (a) Schematic of the battery configuration with ZIF-8/PDA@PP separator and the corresponding battery assembly; (b) TEM image of ZIF-8/PDA; (c) SEM image of ZIF-8/PDA@PP; (d) and (e) the cross-sectional SEM images of ZIF-8/PDA@PP and the corresponding (f) mapping and (g) elemental line scan of Zn.

stability and electrolyte wettability. The Li-S batteries assembled with a modification separator show better cycling performance. The capacity at 2 C remains at 711 mAh·g^{-1} after 500 cycles, and the capacity attenuation per cycle was as low as 0.013%. For the lithium anode, the separator can provide a high lithium ion transference number of 0.88 and homogenize the lithium ion flux. The lithium symmetrical battery is cycled for 1,000 h at the current of 2 mA·cm^{-2} (2 mAh·cm^{-2}) with a small plating/stripping overpotential of 20 mV.

2 Experimental section

Chemicals and materials: All chemicals were used as received without purification. $Zn(NO_3)_2{\cdot}6H_2O$ (99%), $Co(NO_3)_2{\cdot}6H_2O$ (99%) and 2-methylimidazole were purchased from Aladdin. 1,3-Dioxlane (DOL) (99.5%), 1,2-dimethoxyethane (DME) (99.5%), $LiNO_3$ (99.9%), Li_2S and sublimed sulfur power were purchased from Alfa Aesar. Graphene oxide suspension was synthesized by Hummer's method using natural flake graphite [1, 2].

Preparation of PDA@PP: 1 mL Tris-HCl buffer was added into 100 mL deionized water to adjust pH to 8.5, and then 200 mg dopamine was added to solution under stirring. After washed with ethanol, the commercial PP separator was immersed in dopamine hydrochloride solution for 24 h. The polymerization was ended by taking the sample out and washed by ethanol and deionized water for three times respectively.

Preparation of ZIF-8/PP and ZIF-8/PDA@PP: 1.213 g dimethylimidazole and 1.195 g zinc nitrate was dissolved in 20 mL methanol respectively. The synthesized PDA@PP were put into the dimethylimidazole solution and then zinc nitrate solution was slowly added dropwise until the solution turned into a white suspension. After standing for 24 h, the separator was ultrasonically cleaned with ethanol for 30 s. ZIF-8/PP and ZIF-8/PDA@PP were obtained by drying at room temperature overnight.

Preparation of ZIF-8/PDA: 1 mL Tris-HCl buffer was added into 100 mL deionized water to adjust pH to 8.5, and then 200 mg dopamine was added to solution under stirring, which was then centrifuged after standing for 24 h to obtain PDA. Then ZIF-8/PDA@PP was used for the preparation of ZIF-8/PDA by replacing PDA@PP with PDA. Finally, the reacted solution was centrifuged and dried to obtain ZIF-8/PDA powder.

Preparation of the S/rGO cathode: 2 mg of graphene oxide, 1 mol·L^{-1} sodium thiosulfate and 2 mol·L^{-1} hydrochloric acid were mixed in deionized water to obtain 2 mL solution in a vial. After reacted at 95 °C for 2 h, the obtained hydrogel was washed for 3 times by deionized water and then freeze-dried to get the freestanding S/rGO composite. The areal loading of S/rGO depends on the molar mass of sodium thiosulfate and hydrochloric acid. The sulfur content in S/rGO is 80%, and the sulfur loading is 2.5 mg·cm^{-2} for the routine electrochemical performance test. The preparation of high sulfur loading cathodes only requires increasing the amount of sodium thiosulfate.

Materials characterization: Scanning electron microscopic (SEM) images were collected using a JEOL JSM-7100F, which can also provide energy dispersive X-ray spectrometer (EDS) spectra. X-ray diffraction (XRD) measurements were carried out to perform crystallographic structural analysis of electrodes on a D8 Advance X-ray diffractometer. Transmission electron microscopy (TEM) and X-ray photoelectron spectroscopy (XPS) were performed using a Titan G2 60-300 and a VG MultiLab 2000 instrument, respectively. The temperature distribution image was obtained by the thermal imaging camera.

Separator characterization: The chemical composition of the separators was determined by Fourier transform infrared spectroscopy (FT-IR) as well as Raman using a Renishaw Raman spectroscopy system and a Nicolet IS5 spectrometer (Thermo Fisher Scientific Inc.). The dynamic contact angle measurements were conducted using an optical contact angle measuring and contour analysis system (Dataphysics DCA 35). The heat resistance of the separator was proved by an infrared thermal imaging camera (FLIR T429) with a temperature range from 25 to 120 °C.

Electrochemical measurement: CR2025 type coin cells were assembled in an argon filled glovebox. And the contents of water and oxygen were both below 0.1 ppm. The rGO-S samples with a sulfur loading about 0.9 mg were directly used as the cathode, and lithium foil was used as the anode. The used electrolyte was a solution of 1 M Li bistrifluoromethane-sulfonimide (LiTFSI) (DME:DOL) (DME = 1,2-dimethoxyethane and DOL = 1,3-dioxolane, 1:1 by volume) with 1 wt.% $LiNO_3$. The ratio of electrolyte to S is 20 (μL):1 (mg). The cycling tests were performed at a low current density for initial few cycles. The Galvanostatic charge/discharge cycling was carried out in a CT 2001A multichannel battery testing system (Wuhan LAND Electronic Co., Ltd.) with a potential range of 1.6–2.8 V vs. Li/Li$^+$. Galvanostatic Li stripping/plating cycle was performed on the Li/separator/Li at a current density of 2 mA·cm^{-2} with a deposition capacity of 2 mAh·cm^{-2}.

The constant step potential of the electrochemical workstation was set to 10 mV, and the number of lithium ion transfers in different separators was measured with the timing rate. The lithium-ion transference number was calculated from the ratio of steady state current to initial state current according to the following equation:

$$t_{Li}^{+} = \frac{I^{SS}R_b^{SS}(\Delta V - I^0 R_i^0)}{I^0 R_b^0(\Delta V - I^{SS}R_i^{SS})} \quad (1)$$

where t_{Li}^{+} is transference number; ΔV is the polarization voltage (10 mV); while I^{SS} and I^0 represent the current at the steady state and initial state, respectively. Meanwhile, the initial and steady-state values of the bulk resistances (R_b^{SS} and R_b^0, respectively) and electrode/electrolyte interfacial resistances (R_i^{SS} and R_i^0) were measured by EIS before and after the potentiostatic polarization.

3 Results and discussion

First, the ZIF-8 modified layer was prepared on the PP separator that was not modified with PDA with only a few ZIF-8 particles appearing on the ZIF-8/PP separator, while a large number of pores of the separator were still exposed (Fig. S1 in the Electronic Supplementary Material (ESM)). PDA is supposed to be able to bridge PP and MOF by the combination of catechol and zinc ion. The separator pretreated by dopamine could form a PDA layer on the surface of PP (defined as PDA@PP) [36]. The polymerization mechanism of polydopamine is shown in Fig. S2 in the ESM, which can be found that the functionalization of the separator surface would generate abundant functional groups to provide coordination sites for the growth of ZIF-8 [37]. According to the optical photos of the modified PDA separator and pure PP separator (Figs. S3(a) and S3(b) in the ESM), it can be clearly observed that the separator changes from white to dark brown. According to the SEM images (Figs. S3(c) and S3(d) in ESM), the surface morphology of the PDA@PP separator does not show significant changes, but some of the narrow pores are blocked, which is due to the grown PDA layer with thickness less than 50 nm [38]. A new scheme is proposed to bind the modification layer to the separator, in which the carboxyl group in PDA is closely bound to the unsaturated Zn ion in ZIF-8, thereby greatly improving the stability of the modification layer. From the TEM

image (Fig. 1(b)), it can be seen that the particle size of *in-situ* grown ZIF-8 particle is about 100 nm, and the ZIF-8 particles have an intact dodecahedron structure, which are tightly combined with each other by PDA. Analysis combined with the SEM image of the ZIF-8/PDA@PP separator (Fig. 1(c)) shows that the ZIF-8 particles grown on the surface of PDA@PP separator are uniform and form a tightly modification layer that will not fall off easily. The close packing of ZIF-8 particles well covers the pores on the separator surface, which plays a role in physically blocking the shuttle of polysulfides. According to the cross-sectional SEM image, it could be seen that the thickness of the modification layer is about 400 nm (Fig. 1(d)), and small ZIF-8 particles have grown inside the separator. In the near surface area (Fig. S4(a) in the ESM), the layered separator is obviously filled with the ZIF-8 particles. The number of ZIF-8 particles is greatly reduced in the central part of the separator (Fig. S4(b) in the ESM)), while some particles could still be observed. The EDS mapping shown in Fig. 1(f) reveals the sectional distribution of Zn element. It could be observed that there is a general distribution of Zn in the entire cross section, and the Zn content in the middle of the separator is less. The line scanning result (Fig. 1(g)) shows the same gradient distribution of Zn element in the separator, which is consistent with the trend of the concentration distribution of polysulfides [39]. This separator structure provides efficient and continuous chemical adsorption, and the densely distributed ZIF-8 particles on the surface of the separator close to the anode can block polysulfides again.

By comparing the FT-IR spectra of PP, PDA@PP and ZIF-8/PDA@PP (Fig. 2(a)), it is obvious that there are two typical absorption peaks at 1,605 and 1,509 cm^{-1} in the FT-IR spectra of PDA@PP and ZIF-8/PDA@PP. These two peaks are attributed to the stretching vibration of the indole or indole group in the PDA [40], but the 1,509 cm^{-1} peak produces a small-range peak shift due to its combination with the substrate [41]. After combining with ZIF-8, the peak at 1,605 cm^{-1} splits into 1,595 and 1,635 cm^{-1}, which is attributed to the interaction between Zn and PDA [41]. Raman spectroscopy analysis further supports the successful formation of the PDA layer on the PP separator (Fig. S5 in the ESM). Two clear peaks assigned to 1,408 and 1,546 cm^{-1} are derived from the aromatic rings of PDA. Therefore, it is concluded that PP separator was successfully modified with PDA, and the connection between ZIF-8 and PDA depends on the coupling of Zn and PDA functional groups. As shown in XRD patterns (Fig. 2(b)), compared with the simulated peak position of ZIF-8 [42], the diffraction peaks at 7°, 11°, and 13° can be perfectly matched with the characteristic peaks of ZIF-8. The above results demonstrate that the separator is successfully modified by PDA and ZIF-8.

XPS was used to analyze the surface chemical structure of PP, PDA@PP, and ZIF-8/PDA@PP. By comparing the XPS spectra of the separator modified at different stages in Fig. 2(c), it is clearly found that several new element peaks appear on the spectra of the modification separator. The oxygen element comes from the quinone group of catechol in PDA and ZIF-8 is the only source of Zn element. According to the curve fitting results of the O 1s spectrum of PDA (Fig. 2(d)), the two peaks at ~ 528.5 and ~ 529.8 eV correspond to the carbon–oxygen single bond and the carbon–oxygen double bond of the quinone group in the intermediate 5,6-dihydroxyindoline (DHI) [43], respectively. In the analysis of the O 1s spectrum of PDA@PP, the new peak of ~ 532.16 eV in O 1s spectrum is shown in Fig. 2(e), and the original peak of PDA shifts about 0.3 eV. This is due to the fact that PDA is closely combined with PP by catechol after polymerizing DA monomer. After *in-situ* growth of ZIF-8, the O 1s spectrum of ZIF-8/PDA@PP (Fig. 2(f)) adds a new peak at ~ 534.9 eV, which is attributed to the formation of Zn–O bond [25]. In order to eliminate the interference of other factors, ZIF-8/PDA powder samples were prepared for XPS analysis. In the O 1s spectra of ZIF-8/PDA (Fig. S6 in the ESM), the peak of 532.16 eV produced by the combination of PP and PDA does not appear, but the peak at 534.9 eV is the same as that of ZIF8/PDA@PP. It is proved that catechol in PDA forms a strong chemical bond with Zn atoms in ZIF-8 rather than a simple physical bond, which is consistent with the conclusion of FT-IR.

In order to verify the feasibility and safety of the modification separator in the practical application of Li-S batteries, the physical properties of ZIF-8/PDA@PP need to be characterized by different testing methods. The contact angle test was used to study the effect of the modification layer on the wettability of the electrolyte. As shown in Figs. 3(a) and 3(b), due to the presence of PDA, a large

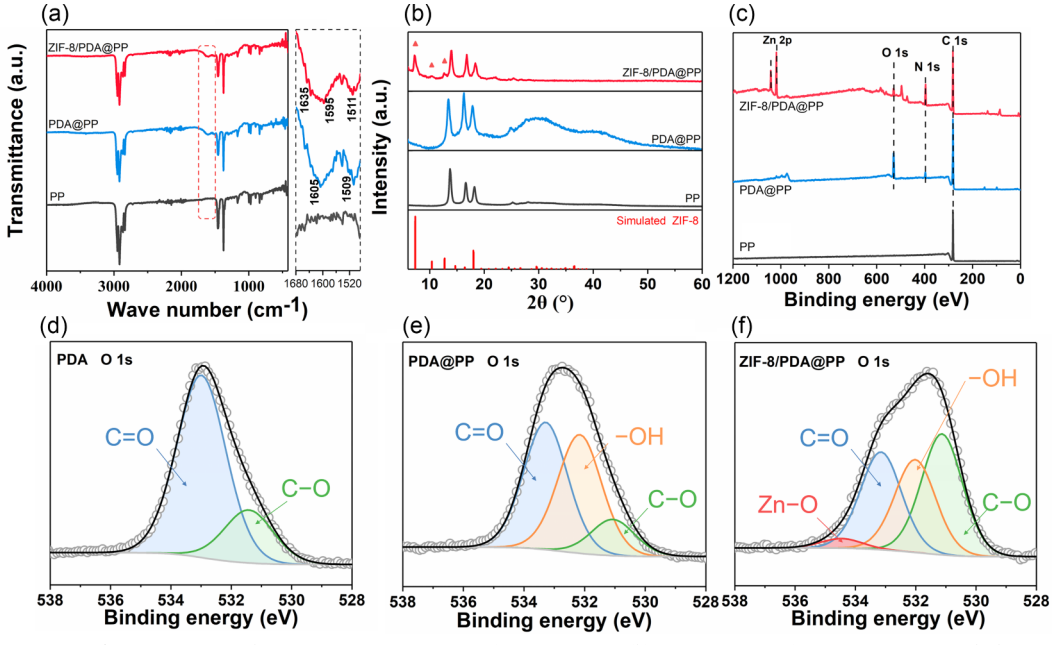

Figure 2 Characterization of PP, PDA@PP and ZIF-8/PDA@PP separator: (a) FT-IR spectra; (b) XRD patterns; (c) XPS survey scans with the corresponding high-resolution scans of O 1s of (d) PP, (e) PDA@PP, and (f) ZIF-8/PDA@PP.

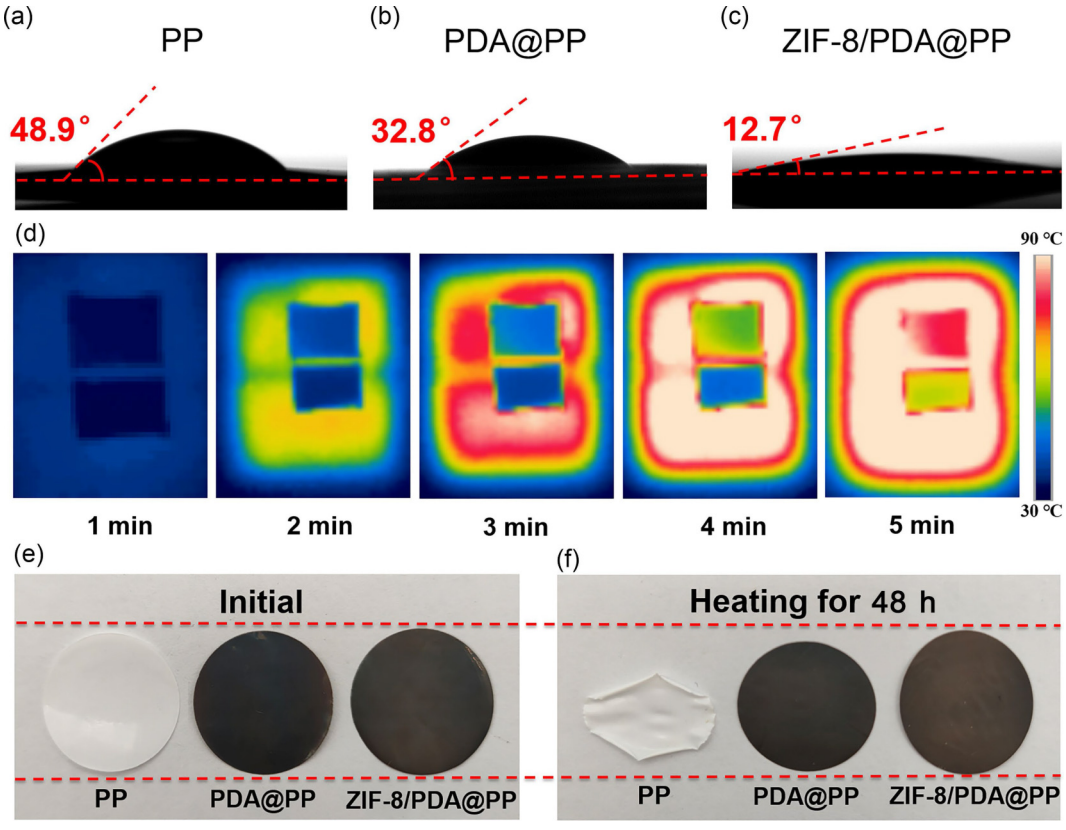

Figure 3 Contact angle measurements with electrolyte for (a) PP separator, (b) PDA@PP separator, (c) ZIF-8/PDA@PP separator; (d) the heat resistance of PP (up) and ZIF-8/PDA@PP (down) separators at 120 °C; (e) and (f) the optical pictures of PP, PDA@PP, ZIF-8/PDA@PP separators before and after thermal treatment at 120 °C for 48 h.

number of polar groups containing ammonia and oxygen were introduced, so that the contact angle was reduced from 48.9° to 32.8°, improving the wettability of the PP surface, thereby increasing the uptake amount of liquid electrolyte. The contact angle was significantly reduced to 12.5° (Fig. 3(c)) when ZIF-8 layer was combined with the same polarity layer, which indicate that ZIF-8/PDA@PP possesses better wettability with the electrolyte. The uniform distribution of electrolyte in the separator is of great significance for the effective transport of lithium ions.

The battery will inevitably generate heat during the cycle, while the shrinkage of the commercial PP separator at high temperature will cause the battery to short circuit. In order to analyze the thermal stability of different separators, the thermal imaging camera was used to analyze the temperature distribution of PP and ZIF-8/PDA@PP under the same heating environment (Fig. 3(d)). After 5 min, the heater was heated to 120 °C, and the temperature of PP separator center was 80 °C, which was higher than the center of ZIF-8/PDA@PP (61 °C). It is found that the surface heat transfer rate of ZIF-8/PDA@PP heated at the same condition is significantly lower than that of PP separator and the ZIF-8/PDA@PP separator has a higher thermal regulation capability. In order to test the heat shrinkage rate, different separators were heated simultaneously at 120 °C for 48 h. It can be seen from Figs. 3(e) and 3(f) in the ESM that PP separator is reduced to nearly half compared with that before heating; the PDA@PP is slightly contracted, while ZIF-8/PDA@PP only begins to show some wrinkle without contraction after 48 h. In general, it is concluded that the modification coating reduces the thermal conductivity of the separator. ZIF-8/PDA@PP possesses higher thermal stability, and it will respond to the temperature more slowly, which improves the safety of Li-S batteries at high temperatures.

Previous studies have shown that the metal sites in the MOF material play a role in promoting lithium ion transmission. In order to verify that the in-situ grown ZIF-8 on the PP separator still retains this characteristic, the current time curve of lithium symmetric batteries were tested to calculate the lithium ion transference numbers. Figures 4(a)–4(c) exhibit the I-t curves of different separators after a 10 mV polarization. After calculation, the lithium ion transference number of ZIF-8/PDA@PP is as high as 0.88, much higher than that of PP (0.72). The results indicates that the dense modification layer on ZIF-8/PDA@PP does not affect the passage of lithium ions. The improvement of electrolyte infiltration and the promotion of polar substances in ZIF-8 on battery dynamics makes the lithium ion transport faster. EIS was used to characterize the internal resistance and charge transfer process. In the Nyquist diagram (Fig. 4(d)), the charge transfer resistance of ZIF-8 (126 Ω) is much lower than that of the PP separator (283 Ω), which means that the battery composed of the modification separator has a smaller electrochemical reaction resistance to promote the charge transfer of the entire battery system.

In order to evaluate the effect of ZIF-8/PDA@PP separator on the inhibition of polysulfides shuttle, a series of electrochemical performance characterization were carried out. Figure 5(a) shows the rate performance of batteries assembled with PP, PDA@PP, and ZIF-8/PDA@PP separators at different rates (0.2, 0.5, 1, 2, and 3 C). The initial capacities of PP, PDA@PP and ZIF-8/PDA@PP at 0.2 C were 1,246, 1,318 and 1,329 mAh·g^{-1}, respectively. However, when the current density increases to 3 C, the ZIF-8/PDA@PP also maintains a capacity of 622 mAh·g^{-1}, whereas the PP separator and the PDA@PP only provide capacities of 223 and 361 mAh·g^{-1}, respectively. The results clearly indicate that ZIF-8/PDA@PP can significantly accelerate reaction kinetics, thus improving the utilization rate of sulfur and the reversible capacity of the battery. In addition, according to the typical charge/discharge voltage curve of Li-S batteries, the conversions of soluble lithium polysulfides (Li_2S_n, $4 < n \leq 8$) and insoluble lithium

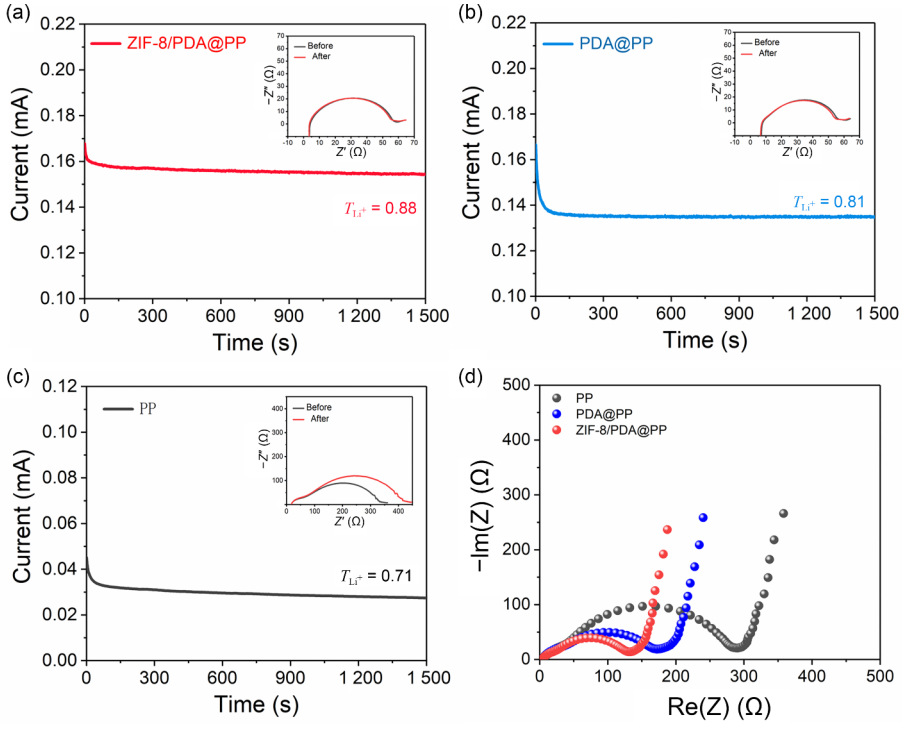

Figure 4 *I–t* curves of different separators after applying a 10 mV polarization: (a) ZIF-8/PDA@PP, (b) PDA@PP and (c) PP. The insets are the corresponding impedance spectra. (d) EIS spectra for the Li-S cells with different separators.

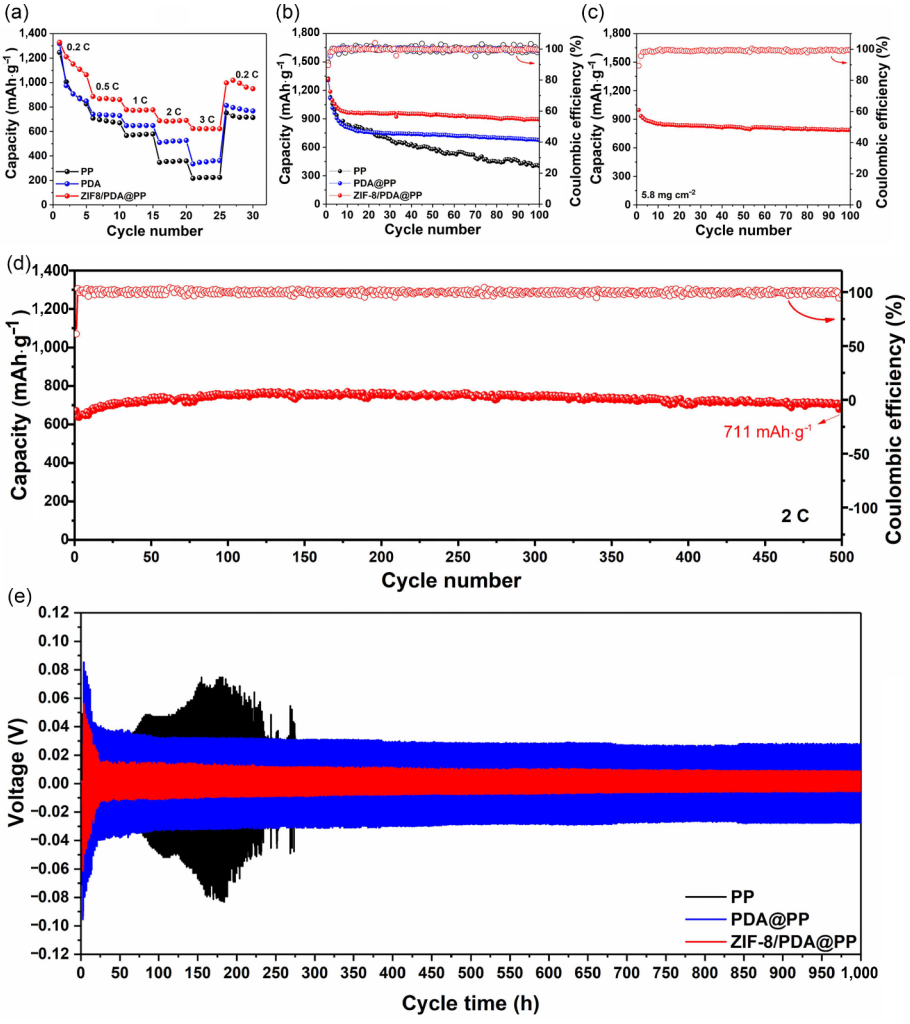

Figure 5 Electrochemical performances of different separators. (a) Rate performances; (b) cycling performance at 0.5 C for 100 cycles; (c) cycling performance of ZIF-8/PDA@PP separator with a high areal sulfur loading of 5.8 mg·cm^{-2}; (d) cycling stability of the ZIF-8/PDA@PP separator at 2 C for 500 cycles; (e) galvanostatic cycling of lithium symmetrical battery at 2 mA·cm^{-2} (2 mAh·cm^{-2}).

polysulfides (Li_2S_2 and Li_2S) correspond to two platforms of 2.3 and 2.1 V, respectively. The platform of ZIF-8/PDA@PP is near 2.3 and 2.1 V (Fig. S7 in the ESM), and the polarization potential is 140 mV, which is much lower than the polarization potential of PP (24 mV). This indicates that ZIF-8/PDA@PP can make the conversion of polysulfides faster, which is beneficial to reducing the sulfur consumption and improving the reversible capacity of the battery. Comparing the voltage plateau changes at different rates (Fig. S8 in the ESM), we can also conclude that the ZIF-8/PDA@PP separator has better cycling stability. At the same time, visual experiments were used for further confirmation (Fig. S9 in the ESM). In 2 h, the Li_2S_6 solution passes through the PP separator to the electrolyte side, while the ZIF-8/PDA@PP separator can still block the shuttle of the polysulfides after 12 h.

In order to fully demonstrate the advantages of ZIF-8/PDA@PP separator, the effects of different separators on the cycling performance of Li-S batteries were further studied. Figure 5(b) shows the cycle curves of the batteries with different separators at 0.5 C. As can be seen from the curves, the capacities of PP, PDA@PP and ZIF-8/PDA@PP can maintain 30%, 52% and 68%, respectively. Considering that high capacity is an indispensable direction for the commercialization of Li-S batteries, it is necessary to test the performance of ZIF/PDA@PP with a high sulfur loading cathode. As shown in Fig. 5(c), even at a high loading of 5.8 mg·cm^{-2}, the initial area specific capacity of the battery is up to 5.78 mAh·cm^{-2} and still retains 82% of capacity after 100 cycles.

The long-term cycle performance of the battery with ZIF-8/PDA@PP was tested at 2 C. As shown in Fig. 5(d), ZIF-8/PDA@PP still has a reversible capacity of 711 mAh·g^{-1}, and the capacity damping per cycle is only 0.013% after 500 cycles. The result proves that the modification separator significantly improves the stability of the positive electrode. In addition, the stability of the negative electrode is also an extremely important part of the battery performance. We have verified this result through tests. It can also be seen from the voltage curve of the lithium symmetric battery in Fig. 5(e), for the PP separator, the overpotential of electroplating/stripping is initially maintained at 32 mV (vs Li^+/Li), and then gradually increases to 58 mV. After 75 h, a large voltage fluctuation occurs, while PDA@PP and ZIF-8/PDA@PP are stable at about 29 and 20 mV after 1,000 h, respectively. The addition of PDA can improve the wettability of the separator and enhance the uptake capability of the liquid electrolyte, which facilitate a well-distributed Li ionic flux over the entire Li-metal area during cycling and therefore lessen Li-dendrite growth. Besides, the strong adhesive interactions of PDA onto Li metal can relieve the local surface tension of the Li metal efficiently and enhance the cycling efficiency of Li-metal anodes immensely [25]. The SEM images of the lithium foil after cycling (Fig. S10 in the ESM) also show that the anode surfaces are smooth with the PDA@PP and ZIF-8/PDA@PP separators. While the formation of uneven dendrites can be clearly seen on the surface of the lithium sheet in the battery using PP separator. This result further demonstrates the homogenization effect of the ZIF-8/PDA@PP modification layer on lithium ion deposition.

4 Conclusion

In conclusion, the robust ZIF-8 modification layer on PP separator was prepared by *in-situ* growth in liquid, and the thickness of the dense layer is only 400 nm. The dense ZIF-8 modification layer and abundant unsaturated metal sites provide a strong physical barrier and chemical adsorption effect on polysulfides, which absorb the shuttle effect of polysulfides effectively. And because of the synergetic effect of ZIF-8 and PDA, it promotes lithium ion transmission, homogenizes lithium ion deposition, and improves the physical properties of the separator and the battery cycle performance. Highly reversible discharge capacities of 893 mAh·g^{-1} could be obtained at 0.5 C for 100 cycles. It also delivered excellent capacity retention of 711 mAh·g^{-1} after 500 cycles at 2 C. Besides, the ZIF-8/PDA@PP separator retains 82% of capacity at 0.2 C after 100 cycles with a high sulfur loading of 5.8 mg·cm^{-2}. This work provides a novel idea for the combination mode between modification layers and separators. The method proposed in this work possesses the advantages of low cost and simple synthesis route, and it can be extended to a variety of separators and various MOF materials for modification. The MOF material used is not limited to ZIF-8, so it has a wide range of applications.

Acknowledgements

This work was supported by China-Japanese Research Cooperative Program founded by the Ministry of Science and Technology of the People's Republic of China (No. 2017YFE0127600), the National Natural Science Foundation of China (No. 51702247), the Fundamental Research Funds for the Central Universities (No. WUT: 2020III023, 2020III050, 2021IVA123, 2021III009), Hainan Provincial Joint Project of Sanya Yazhou Bay Science and Technology City (No. 520LH056), Sanya Science and Education Innovation Park of Wuhan University of Technology (No. 2020KF0021), and the State Key Laboratory of Advanced Technology for Materials Synthesis and Processing (WUT: 2021-ZD-1).

Electronic Supplementary Material: Supplementary material (further details of SEM imaging and Raman spectroscopy measurements) is available in the online version of this article at https://doi.org/10.1007/s12274-022-4423-2.

References

[1] Tarascon, J. M.; Armand, M. Issues and challenges facing rechargeable lithium batteries. *Nature* **2001**, *414*, 359–367.

[2] Seh, Z. W.; Sun, Y. M.; Zhang, Q. F.; Cui. Y. Designing high-energy lithium-sulfur batteries. *Chem. Soc. Rev.* **2016**, *45*, 5605–5634.

[3] Zhao, M.; Peng, Y. Q.; Li, B. Q.; Zhang, X. Q.; Huang, J. Q. Regulation of carbon distribution to construct high-sulfur-content cathode in lithium-sulfur batteries. *J. Energy Chem.* **2021**, *56*, 203–208.

[4] Kim, H.; Jeong, G.; Kim, Y. U.; Kim, J. H.; Park, C. M.; Sohn, H. J. Metallic anodes for next generation secondary batteries. *Chem. Soc. Rev.* **2013**, *42*, 9011–9034.

[5] Zhao, M.; Li, X. Y.; Chen, X.; Li, B. Q.; Kaskel, S.; Zhang, Q.; Huang, J. Q. Promoting the sulfur redox kinetics by mixed organodiselenides in high-energy-density lithium-sulfur batteries. *eSience* **2021**, *1*, 44–52.

[6] Liu, X.; Huang, J. Q.; Zhang, Q.; Mai, L. Nanostructured metal oxides and sulfides for lithium-sulfur batteries. *Adv. Mater.* **2017**, *29*, 1601759.

[7] Pang, Q.; Liang, X.; Kwok, C. Y.; Nazar, L. F. Advances in lithium-sulfur batteries based on multifunctional cathodes and electrolytes. *Nat. Energy* **2016**, *1*, 16132.

[8] Tao, T.; Lu, S. G.; Fan, Y.; Lei, W. W.; Huang, S. M.; Chen, Y. Anode improvement in rechargeable lithium-sulfur batteries. *Adv. Mater.* **2017**, *29*, 1700542.

[9] Huang, J. Q.; Zhang, Q.; Peng, H. J.; Liu, X. Y.; Qian, W. Z.; Wei, F. Ionic shield for polysulfides towards highly-stable lithium-sulfur batteries. *Energy Environ. Sci.* **2014**, *7*, 347–353.

[10] Ryou, M. H.; Lee, Y. M.; Park, J. K.; Choi, J. W. Mussel-inspired polydopamine-treated polyethylene separators for high-power Li-ion batteries. *Adv. Mater.* **2011**, *23*, 3066–3070.

[11] Ryou, M. H.; Lee, D. J.; Lee, J. N.; Lee, Y. M.; Park, J. K.; Choi, J. W. Excellent cycle life of lithium-metal anodes in lithium-ion

batteries with mussel-inspired polydopamine-coated separators. *Adv. Energy Mater.* **2012**, *2*, 645–650.
[12] Kim, J. H.; Lee, D.; Lee, Y. H.; Chen, W. S.; Lee, S. Y. Nanocellulose for energy storage systems: Beyond the limits of synthetic materials. *Adv. Mater.* **2019**, *31*, 1804826.
[13] Yu, X. W.; Wu, H.; Koo, J. H.; Manthiram, A. Tailoring the pore size of a polypropylene separator with a polymer having intrinsic nanoporosity for suppressing the polysulfide shuttle in lithium-sulfur batteries. *Adv. Energy Mater.* **2020**, *10*, 1902872.
[14] Wang, X. F.; Wang, Z. X.; Chen, L. Q. Reduced graphene oxide film as a shuttle-inhibiting interlayer in a lithium-sulfur battery. *J. Power Sources* **2013**, *242*, 65–69.
[15] Pang, Y.; Wei, J. S.; Wang, Y. G.; Xia, Y. Y. Synergetic protective effect of the ultralight MWCNTs/NCQDs modified separator for highly stable lithium-sulfur batteries. *Adv. Energy Mater.* **2018**, *8*, 1702288.
[16] Li, Z. H.; Zhou, C.; Hua, J. H.; Hong, X. F.; Sun, C. L.; Li, H. W.; Xu, X.; Mai, L. Engineering oxygen vacancies in a polysulfide-blocking layer with enhanced catalytic ability. *Adv. Mater.* **2020**, *32*, 1907444.
[17] Tan, S. S.; Dai, Y. H.; Jiang, Y. L.; Wei, Q. L.; Zhang, G. B.; Xiong, F. Y.; Zhu, X. Q.; Hu, Z. Y.; Zhou, L.; Jin, Y. C. et al. Revealing the origin of highly efficient polysulfide anchoring and transformation on anion-substituted vanadium nitride host. *Adv. Funct. Mater.* **2021**, *31*, 2008034.
[18] He, J. R.; Chen, Y. F.; Manthiram, A. Vertical Co_9S_8 hollow nanowall arrays grown on a Celgard separator as a multifunctional polysulfide barrier for high-performance Li-S batteries. *Energy Environ. Sci.* **2018**, *11*, 2560–2568.
[19] Xu, J.; An, S. H.; Song, X. Y.; Cao, Y. J.; Wang, N.; Qiu, X.; Zhang, Y.; Chen, J. W.; Duan, X. L.; Huang, J. H. et al. Towards high performance Li-S batteries via sulfonate-rich COF-modified separator. *Adv. Mater.* **2021**, *33*, 2105178.
[20] Meng, J. S.; Liu, X.; Niu, C. J.; Pang, Q.; Li, J. T.; Liu, F.; Liu, Z. A.; Mai, L. Advances in metal-organic framework coatings: Versatile synthesis and broad applications. *Chem. Soc. Rev.* **2020**, *49*, 3142–3186.
[21] Zhou, C.; Li, Z. H.; Xu, X.; Mai, L. Q. Metal-organic frameworks enable broad strategies for lithium-sulfur batteries. *Natl. Sci. Rev.* **2021**, *8*, nwab055.
[22] Jeong, Y. C.; Kim, J. H.; Nam, S.; Park, C. R.; Yang, S. J. Rational design of nanostructured functional interlayer/separator for advanced Li-S batteries. *Adv. Funct. Mater.* **2018**, *28*, 1707411.
[23] Lin, C.; Qu, L. B.; Li, J. T.; Cai, Z. Y.; Liu, H. Y.; He, P.; Xu, X.; Mai, L. Porous nitrogen-doped carbon/MnO coaxial nanotubes as an efficient sulfur host for lithium sulfur batteries. *Nano Res.* **2019**, *12*, 205–210.
[24] Mathew, D. E.; Gopi, S.; Kathiresan, M.; Rani, G. J.; Thomas, S.; Stephan, A. M. A porous organic polymer-coated permselective separator mitigating self-discharge of lithium-sulfur batteries. *Mater. Adv.* **2020**, *1*, 648–657.
[25] He, M. L.; Wang, L.; Lv, Y. T.; Wang, X. D.; Zhu, J. N.; Zhang, Y.; Liu, T. T. Novel polydopamine/metal organic framework thin film nanocomposite forward osmosis membrane for salt rejection and heavy metal removal. *Chem. Eng. J.* **2020**, *389*, 124452.
[26] Ma, C. C.; Li, Y. J.; Nian, P.; Liu, H. Q.; Qiu, J. S.; Zhang, X. F. Fabrication of oriented metal-organic framework nanosheet membrane coated stainless steel meshes for highly efficient oil/water separation. *Sep. Purif. Technol.* **2019**, *229*, 115835.
[27] Zhao, Y. H.; Dong, H. X.; He, X. Y.; Yu, J.; Chen, R. R.; Liu, Q.; Liu, J. Y.; Zhang, H. S.; Li, R. M.; Wang, J. Design of 2D mesoporous Zn/Co-based metal-organic frameworks as a flexible electrode for energy storage and conversion. *J. Power Sources* **2019**, *438*, 227057.
[28] Pan, T. Y.; Li, Z. H.; He, Q.; Xu, X.; He, L.; Meng, J. S.; Zhou, C.; Zhao, Y.; Mai, L. Uniform zeolitic imidazolate framework coating via *in situ* recoordination for efficient polysulfide trapping. *Energy Storage Mater.* **2019**, *23*, 55–61.
[29] Xia, Y. Y.; Xu, N.; Du, L. L.; Cheng, Y.; Lei, S. L.; Li, S. J.; Liao, X. B.; Shi, W. C.; Xu, L.; Mai, L. Rational design of ion transport paths at the interface of metal-organic framework modified solid electrolyte. *ACS Appl. Mater. Interfaces* **2020**, *12*, 22930–22938.
[30] Zhuang, T. Z.; Huang, J. Q.; Peng, H. J.; He, L. Y.; Cheng, X. B.; Chen, C. M.; Zhang, Q. Rational integration of polypropylene/graphene oxide/nafion as ternary-layered separator to retard the shuttle of polysulfides for lithium-sulfur batteries. *Small* **2016**, *12*, 381–389.
[31] Zhou, G. M.; Li, L.; Wang, D. W.; Shan, X. Y.; Pei, S. F.; Li, F.; Cheng, H. M. A flexible sulfur-graphene-polypropylene separator integrated electrode for advanced Li-S batteries. *Adv. Mater.* **2015**, *27*, 641–647.
[32] Bai, S. Y.; Liu, X. Z.; Zhu, K.; Wu, S. C.; Zhou, H. S. Metal-organic framework-based separator for lithium-sulfur batteries. *Nat. Energy* **2016**, *94*, 16094.
[33] Wang, J.; Wang, K.; Yang, Z.; Li, X. D.; Gao, J.; He, J. J.; Wang, N.; Wang, H. L.; Zhang, Y. L.; Huang, C. S. Effective stabilization of long-cycle lithium-sulfur batteries utilizing *in situ* prepared graphdiyne-modulated separators. *ACS Sustainable Chem. Eng.* **2020**, *8*, 1741–1750.
[34] Li, W. B.; Su, P. C.; Li, Z. J.; Xu, Z. H.; Wang, F.; Ou, H. S.; Zhang, J. H.; Zhang, G. L.; Zeng, E. Ultrathin metal-organic framework membrane production by gel-vapour deposition. *Nat. Commun.* **2017**, *8*, 406.
[35] Zhou, C.; He, Q.; Li, Z. H.; Meng, J. S.; Hong, X. F.; Li, Y.; Zhao, Y.; Xu, X.; Mai, L. Q. A robust electrospun separator modified with *in situ* grown metal-organic frameworks for lithium-sulfur batteries. *Chem. Eng. J.* **2020**, *395*, 124979.
[36] Delparastan, P.; Malollari, K. G.; Lee, H.; Messersmith, P. B. Direct evidence for the polymeric nature of polydopamine. *Angew. Chem., Int Ed.* **2019**, *58*, 1077–1082.
[37] Lee, H. A.; Park, E.; Lee, H. Polydopamine and its derivative surface chemistry in material science: A focused review for studies at KAIST. *Adv. Mater.* **2020**, *32*, 1907505.
[38] D'Ischia, M.; Napolitano, A.; Ball, V.; Chen, C. T.; Buehler, M. J. Polydopamine and eumelanin: From structure-property relationships to a unified tailoring strategy. *Acc. Chem. Res.* **2014**, *47*, 3541–3550.
[39] Li, Y.; Li, Z. H.; Zhou, C.; Liao, X. B.; Liu, X. W.; Hong, X. F.; Xu, X.; Zhao, Y.; Mai, L. Gradient sulfur fixing separator with catalytic ability for stable lithium sulfur battery. *Chem. Eng. J.* **2021**, *422*, 130107.
[40] Liu, T. Y.; Kim, K. C.; Lee, B.; Chen, Z. M.; Noda, S.; Jang, S. S.; Lee, S. W. Self-polymerized dopamine as an organic cathode for Li- and Na-ion batteries. *Energy Environ. Sci.* **2017**, *10*, 205–215.
[41] Wu, H. Q.; Ang, J. M.; Kong, J. H.; Zhao, C. Y.; Du, Y. H.; Lu, X. H. One-pot synthesis of polydopamine-Zn complex antifouling coatings on membranes for ultrafiltration under harsh conditions. *RSC Adv.* **2016**, *6*, 103390.
[42] Wang, X. P.; Hou, J. W.; Chen, F. S.; Meng, X. M. In-situ growth of metal-organic framework film on a polydopamine-modified flexible substrate for antibacterial and forward osmosis membranes. Sep. Purif. *Technol.* **2020**, *236*, 116239.
[43] Sun, T.; Li, Z. J.; Wang, H. G.; Bao, D.; Meng, F. L.; Zhang, X. B. A biodegradable polydopamine-derived electrode material for high-capacity and long-life lithium-ion and sodium-ion batteries. *Angew. Chem., Int. Ed.* **2016**, *55*, 10662–10666.